catalysts

MDPI

Article

TiO_2/Zeolite Composites for SMX Degradation under UV Irradiation

Saule Mergenbayeva [1], Zhanibek Abitayev [1], Milana Batyrbayeva [1], John Vakros [2], Dionissios Mantzavinos [2], Timur Sh. Atabaev [3] and Stavros G. Poulopoulos [1,*]

[1] Department of Chemical and Materials Engineering, School of Engineering and Digital Sciences, Nazarbayev University, Astana 010000, Kazakhstan; saule.mergenbayeva@nu.edu.kz (S.M.); zhanibek.abitayev@nu.edu.kz (Z.A.); milana.batyrbayeva@nu.edu.kz (M.B.)
[2] Department of Chemical Engineering, University of Patras, University Campus, Caratheodory 1, GR-26504 Patras, Greece; vakros@chemistry.upatras.gr (J.V.); mantzavinos@chemeng.upatras.gr (D.M.)
[3] Department of Chemistry, School of Sciences and Humanities, Nazarbayev University, Astana 010000, Kazakhstan; timur.atabaev@nu.edu.kz
* Correspondence: stavros.poulopoulos@nu.edu.kz; Tel.: +7-7172-694608

Abstract: Sulfamethoxazole (SMX) is a common antibiotic that is considered an emerging pollutant of water bodies, as it is toxic for various aquatic species. TiO_2-based photocatalysis is a promising method for SMX degradation in water. In this work, TiO_2/zeolite (Z-45 loaded with TiO_2 labeled as TZ and ZSM-5 loaded with TiO_2 labeled as TZSM) composites were prepared by mechanical mixing and liquid impregnation methods, and the photocatalytic performance of these composites (200 mg·L^{-1}) was investigated toward the degradation of SMX (30 mg·L^{-1}) in water under UV light (365 nm). The pseudo-first-order reaction rate constant of the TZSM1450 composite was 0.501 min^{-1}, which was 2.08 times higher than that of TiO_2 (k = 0.241 min^{-1}). Complete SMX degradation was observed in 10 min using the UV/TZSM1450 system. The mineralization ability in terms of total organic carbon (TOC) removal was also assessed for all of the prepared composites. The results showed that 65% and 67% of SMX could be mineralized within 120 min of photocatalytic reaction by TZSM2600 and TZSM1450, respectively. The presence of Cl^- and CO_3^{2-} anions inhibited the degradation of SMX, while the presence of NO_3^- had almost no effect on the degradation efficiency of the UV/TZSM1450 system. The electrical energy per order estimated for the prepared composites was in the range of 68.53–946.48 kWh m^{-3} $order^{-1}$. The results obtained revealed that the TZSM1450 composite shows promising potential as a photocatalyst for both the degradation and mineralization of SMX.

Keywords: SMX; TiO_2; Z-45; ZSM-5; UV light; degradation; mineralization

Citation: Mergenbayeva, S.; Abitayev, Z.; Batyrbayeva, M.; Vakros, J.; Mantzavinos, D.; Atabaev, T.S.; Poulopoulos, S.G. TiO_2/Zeolite Composites for SMX Degradation under UV Irradiation. *Catalysts* **2024**, *14*, 147. https://doi.org/10.3390/catal14020147

Academic Editors: Maria Victoria Lopez-Ramon and Ana Paula da Costa Ribeiro

Received: 17 January 2024
Revised: 14 February 2024
Accepted: 14 February 2024
Published: 16 February 2024

1. Introduction

The occurrence of antibiotics in aquatic environments has posed considerable threats to the environment and human health [1,2]. The discharge from wastewater treatment plants (WWTPs) significantly contributes to the presence of these compounds in water, establishing them as a major source of antibiotics in aquatic ecosystems [3,4]. Among various antibiotics, sulfamethoxazole (SMX) is one of the most widespread sulfonamides, mainly applied in human and veterinary medicine to cure bacterial infections [5,6], and therefore has been considered as one of the representatives of antibiotics in livestock wastewater [7]. Due to the incomplete metabolization of SMX by living beings and its high persistence [8], most of the consumed SMX can enter the water systems through excreta [9], eventually threatening aquatic organisms and human health. The concentration of SMX frequently detected in different types of water including wastewater effluent, surface water, and groundwater [10] ranges from ng·L^{-1} to μg·L^{-1} [11,12]. SMX cannot be removed by traditional treatment processes, which is ascribed to its non-biodegradable characteristics [13,14].

Hence, there is a need for an effective method to eliminate it from water. Recently, various approaches have been used to treat SMX-containing wastewater [14].

Heterogeneous photocatalysis has received growing attention for the effective degradation and mineralization of persistent organic pollutants [15,16]. Different catalysts have been investigated to degrade SMX under the use of light irradiation. Among them, titanium dioxide (TiO_2), which is a semiconductor photocatalyst, has a prominent place in photocatalysis [17], since it can decompose toxic organic pollutants in water by generating active species (·OH) with high oxidation potential. Even though TiO_2 possesses chemical stability [18], non-toxicity [19], and low cost [20], its application remains limited. The fabrication of photocatalyst (TiO_2) alongside a material (support) that efficiently adsorbs organic pollutants could be beneficial compared to their separate use because of the reversible transfer of intermediates [21] and reactive radicals between the photocatalyst and the support surface [22]. This composite design could enhance the photocatalytic activity by delocalizing the band gap excited electrons, effectively suppressing the recombination of e^-/h^+ pairs [23,24].

Zeolite is a material with distinctive properties including peculiar ion exchange [25,26], surface acidity, and inexpensive and environmentally benign nature [27,28]. Modifying TiO_2 with zeolites may provide more active surfaces and prevent clotting, significantly improving the photodegradation performance of the catalyst. There are various studies on the application of TiO_2/zeolite composites as a catalyst in photocatalytic reactions in the literature [29,30]. For example, An et al. [31] synthesized carbon doped-TiO_2 coated on zeolites by solid-state dispersion and used it toward the degradation of eighteen pharmaceuticals and pesticides, including SMX. The results showed that the higher adsorption capacity of the zeolite improved the degradation efficiency of the photocatalyst. The study performed by An et al. [31] represents only the degradation of eighteen pharmaceuticals and pesticides, including SMX. Liu et al. [32] reported the successful photocatalytic degradation of sulfadiazine using natural zeolite coated with TiO_2 under UV light irradiation. Zhang et al. [33] prepared a TiO_2/zeolite composite using the hydrolysis deposition technique. The adsorption and catalytic properties of the prepared composites were evaluated in the elimination of gaseous and aqueous organic contaminants. The results revealed that the TiO_2/acid leaching zeolite exhibited higher photodegradation activities than the bare TiO_2 for formaldehyde, phenol, and rhodamine B.

Although several studies have reported the combination of TiO_2 with zeolite, to the best of the authors' knowledge there is no report on the application of such composites for the degradation and mineralization of SMX. To study this prospect, two different synthesis approaches were applied to prepare TiO_2/zeolite (TZ and TZSM) composites, which were used to degrade SMX in water under UV light (365 nm) irradiation. The effect of the presence of various anions in SMX solution on the photocatalytic activity was also investigated for the most efficient composite. Finally, the energy consumption required for the photodegradation of SMX was calculated and compared with the literature.

2. Results

2.1. Characterization

The phase composition of the composites prepared was firstly investigated by XRD analysis, and the results are shown in Figure 1. Distinct diffraction peaks related to the zeolite (Z or ZSM-5) were observed for all composites, regardless of the intensity or the weight fraction of zeolite. The characteristic peaks at 23.0° and 23.8° in TZSM1450 and TZSM2600 represent major ZSM-5 peaks [34,35]. The characteristic peaks of TiO_2 anatase (JCPDS No. 00-021-12-72) at 2θ = 25.3°, 37.8°, 48.0°, 53.9°, 55.1°, 75.2° could be observed in all of the prepared composites, which were ascribed to the (101), (004), (200), (105), (211), and (215) planes, respectively. The intensity of the (101) TiO_2 anatase peak was more intense for TZ2600 and TZSM2600 composites as a result of the weight fraction of TiO_2 dispersed on the surface of the zeolite. In general, the XRD patterns of TZ2600 and TZSM2600 were almost the same as of pure TiO_2. On the other hand, the peaks corresponding to the zeolite

(Z or ZSM-5) were weak, which could be ascribed to the low content of zeolite in the composites and to the fact that the zeolite surface was assembled by TiO_2 nanoparticles, resulting in a decline of zeolite peaks. Similarly, in the pattern of the TZSM1450 composite, the characteristic peaks of TiO_2 were weaker as the content of TiO_2 was lower.

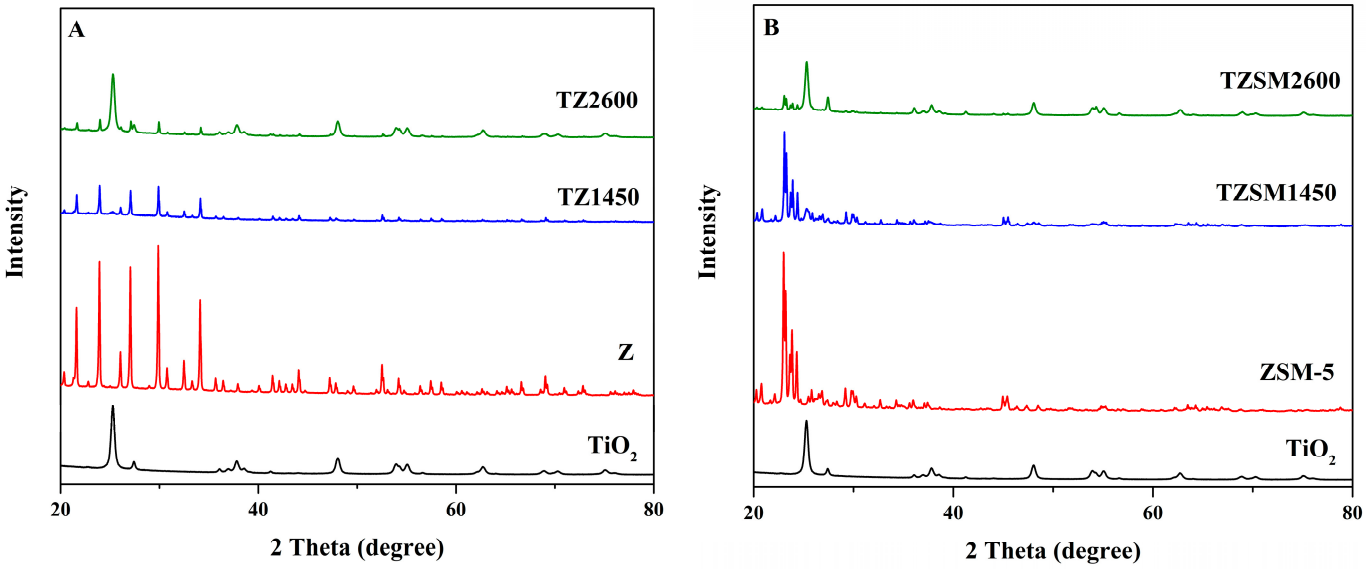

Figure 1. XRD patterns of TZ (**A**) and TZSM (**B**) composites.

In addition to XRD, Raman analysis was implemented to explore the structure and properties of TZ and TZSM composites from their vibrational modes. It can be observed in Figure 2 that all of the composites contained peaks corresponding to TiO_2 anatase centered at 139, 195 (symmetric stretching vibration of O–Ti–O), 393 (symmetrical O–Ti–O bending vibration), 516 (asymmetrical bending vibration), and 635 cm^{-1} (symmetric stretching vibration of O–Ti–O). Also, the high-intensity peak at about 139 cm^{-1} shifted to a higher wavenumber ascribed to the strengthened interaction between TiO_2 and zeolite [36,37].

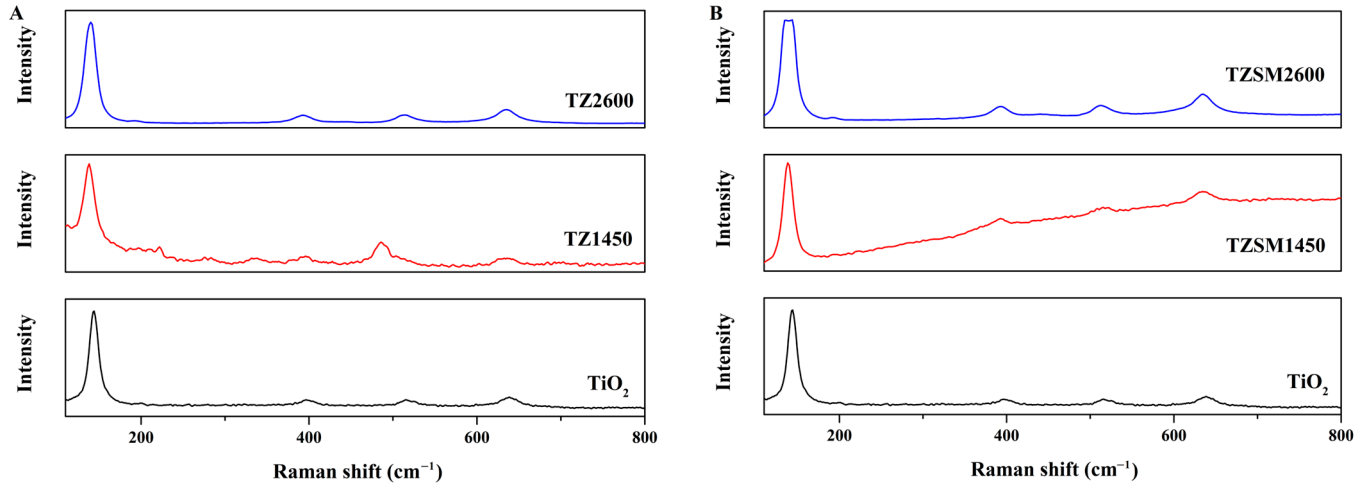

Figure 2. Raman spectra of (**A**) TZ and (**B**) TZSM composites. Different colors were used to distinct pure TiO_2 from synthesized composites (spectra of composites calcined at 450 °C-red, composites calcined at 600 °C-blue).

The morphology of pure zeolites (Z and ZSM-5), as well as of TZ and TZSM composites were examined by SEM (Figures 3 and 4). Both types of zeolites exhibited relatively smooth surfaces, composed of abundant rectangular particles. The SEM image of TZ2600 revealed

that the surface of Z was densely dispersed by TiO_2 nanoparticles. This could be associated with the high content of TiO_2 used in the preparation of these composites, and supported the XRD results regarding the variation in TiO_2/zeolite ratio.

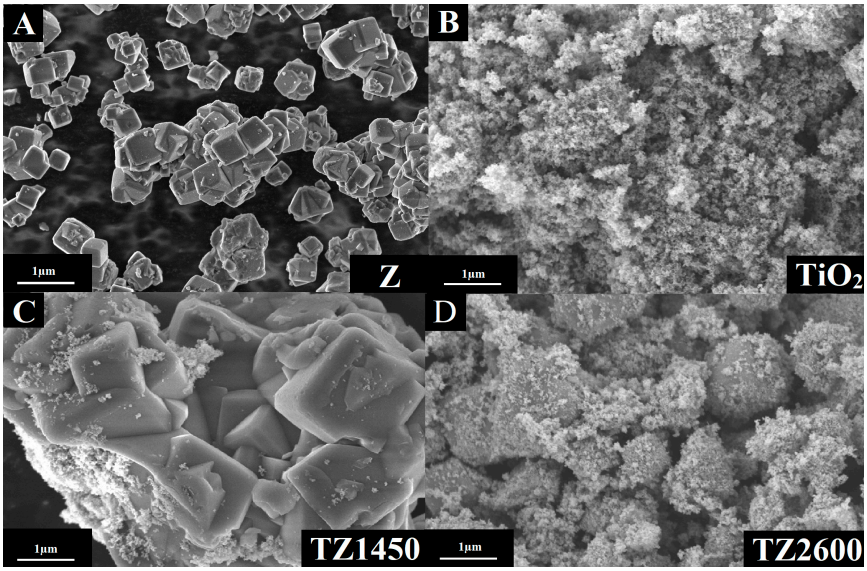

Figure 3. SEM images of (**A**) Z, (**B**) TiO_2, (**C**) TZ1450 and (**D**) TZ2600.

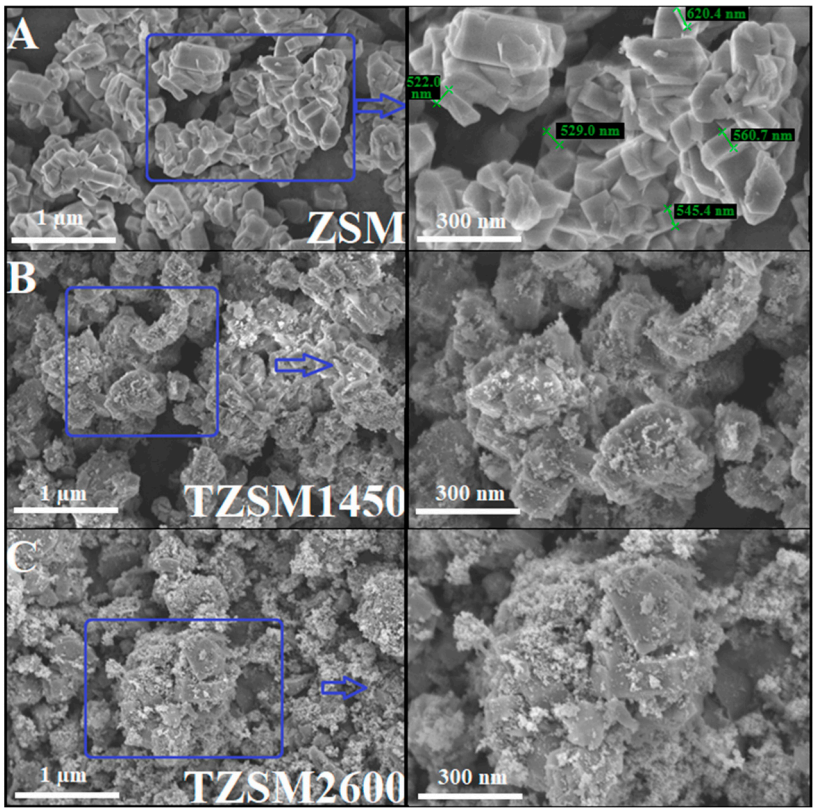

Figure 4. SEM images of (**A**) ZSM-5, (**B**) TZSM1450, and (**C**) TZSM2600 at 1 μm and 300 nm (partially enlarged view).

In comparison with TZ2600, TZSM1450 and TZSM2600 images showed that TiO_2 particles were homogeneously distributed on ZSM-5.

The presence of TiO_2 on the surface of zeolite was confirmed by the EDS technique in all of the prepared composites (Figure 5). The Ti content was higher in TZ2600 and

TZSM2600, which was in accordance with the applied amount of TiO_2. In addition, the Si/Al ratio was calculated for all composites. It can be observed that the Si/Al ratios for TZ1450, TZ2600, TZSM1450, and TZSM2600 composites were about 0.99, 0.91, 18.25, and 18.00, respectively. It has been previously reported that the Si/Al ratio could affect photocatalytic activity. In particular, the increase in the Si/Al ratio could result in an improved photocatalytic activity of the material [38].

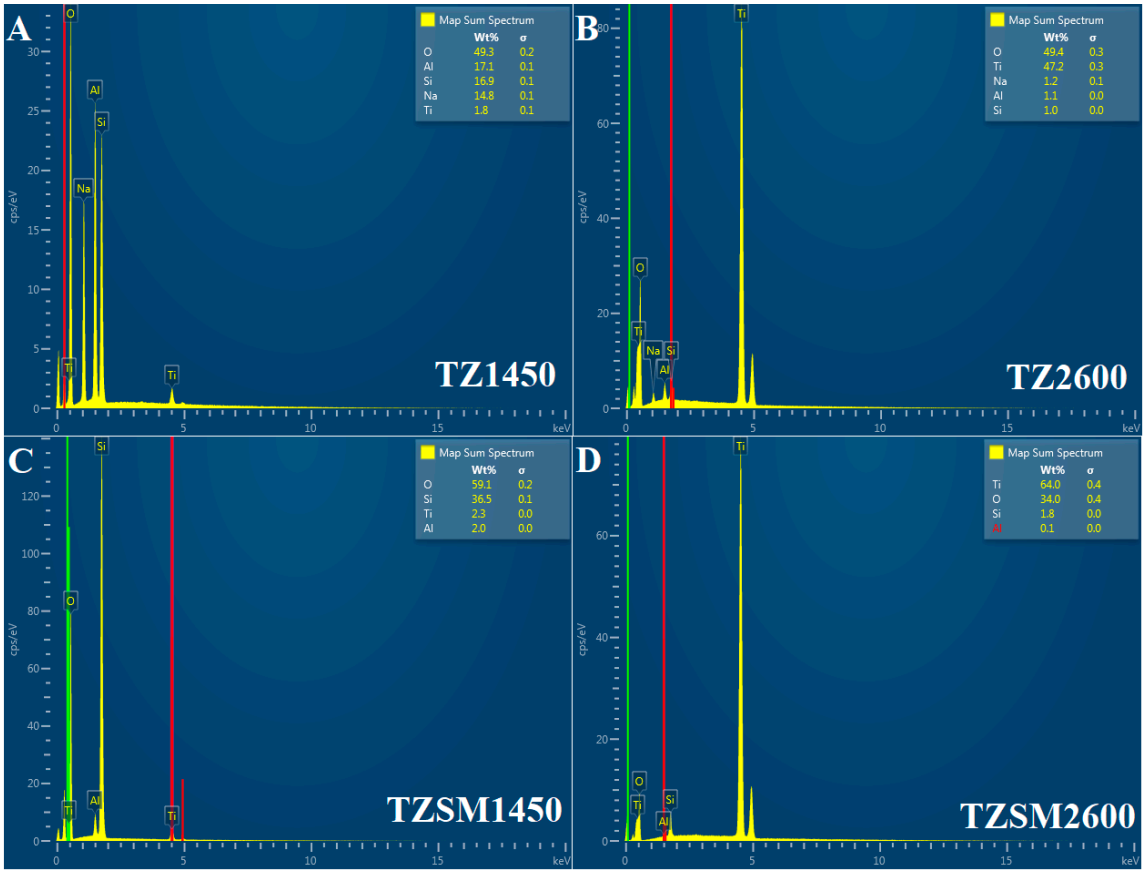

Figure 5. EDS mapping of (**A**) TZ1450, (**B**) TZ2600, (**C**) TZSM1450, and (**D**) TZSM2600 composites.

The light absorption properties of TZ and TZSM composites were examined by UV-Vis Diffuse Reflectance Spectroscopy (DRS). It can be observed that all synthesized composites illustrated strong absorption in the UV region, similar to TiO_2 (Figure 6).

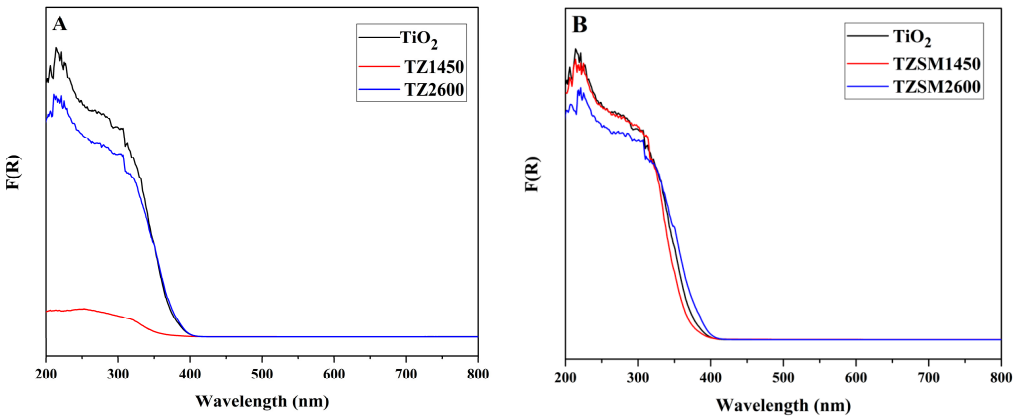

Figure 6. UV-Vis DRS images for prepared (**A**) TZ and (**B**) TZSM composites comparing with TiO_2.

An insignificant reduction in the absorption intensity of the UV region and a slight shift towards higher wavelengths were observed for TZ2600 and TZSM600. However, almost no change was observed for TZSM1450.

The textural properties of the photocatalysts are important for the degradation of a model pollutant. The large specific surface area is especially beneficial through improving the contact probability of the pollutant with the active sites of the material. Table 1 shows the calculated S_{BET} values in relation to the Si/Al ratio. It was observed that the combination of TiO_2 with Z was accompanied by a decrease in S_{BET}, while the introduction of TiO_2 onto ZSM-5 significantly increased the S_{BET} value. This phenomenon could be associated with the loss of the existing micropores at low Si/Al ratios for TZ composites. The findings are consistent with previously reported studies [39,40].

Table 1. The calculated S_{BET} values in relation to Si/Al ratio.

Catalyst	S_{BET} (m^2/g)	Si/Al Ratio
TiO_2	52.4	-
TZ1450	10.7	0.99
TZ2600	47.1	0.91
TZSM1450	361.7	18.25
TZSM2600	109.9	18.00

2.2. Photocatalytic Degradation and Mineralization of SMX

To investigate the photocatalytic activity of TZ and TZSM composites (200 mg·L^{-1}) toward the degradation of SMX (30 mg·L^{-1}), experiments were conducted under UV light irradiation. Before the light exposure, the adsorption performance of the synthesized catalysts was tested. All four catalysts showed insignificant adsorption toward SMX, and the removal efficiencies for TZ2600, TZSM2600, TZ1450, and TZSM1450 were 2.4%, 2.4%, 3.3%, and 6.1%, respectively. The pure TiO_2 adsorbed 3.85% of SMX.

The degradation (%) of SMX was calculated by Equation (1):

$$\text{MX degradation (\%)} = ([SMX]_0 - [SMX]_t)/[SMX]_0 \times 100 \quad (1)$$

where $[SMX]_0$ is the initial SMX concentration in solution; $[SMX]_t$ is the concentration of SMX after a certain reaction time.

A blank experiment of SMX solution exposed to UV light without any catalyst was also performed for comparison. As a result of the blank control experiment, the use of only UV irradiation could degrade up to 70% of SMX, since SMX can absorb UV light and some bonds can be destroyed. Significantly lower degradations of SMX have been previously reported under UVA irradiation as SMX mainly absorbs light until 310 nm [41]. The significant photolysis of SMX could be related to the presence of additional minor wavelengths of irradiation in the UVC region of the lamp used, as no UVC filter was used.

It can be observed from Figure 7A that the TZ2600 composite exhibited the lowest photocatalytic activity, achieving an SMX degradation of about 33%. On the other hand, 100% of SMX was degraded after 10 min of photocatalytic reaction using TZSM1450, which was higher than the degradation achieved with pure TiO_2. This phenomenon could be associated with the fact that zeolite can act as an electron trapper by inhibiting the charge recombination of electron–hole (e^-/h^+) pairs [42]. Therefore, the photo-induced e^- can be transferred to the surface of zeolite or react with dissolved oxygen (O_2) to form the superoxide radical ($O_2^{\cdot-}$), while h^+ at the TiO_2 can react with the adsorbed SMX [43]. This illustrates that zeolite enhances the photocatalytic activity of TiO_2 [44]. The results are in good agreement with the XRD and SEM findings.

In general, the combination of ZSM with TiO_2 showed a more advantageous catalytic effect than the combination of Z with TiO_2. These findings could be associated with the higher Si/Al ratio for TZSM composites that led to enhanced photocatalytic activity.

Although the activity of TZ1450 was higher than that of TZ2600, it was still lower than that of pure TiO_2. Such a behavior could be explained by the deterioration caused by changes in the applied zeolite type, preparation method, and calcination temperature [45].

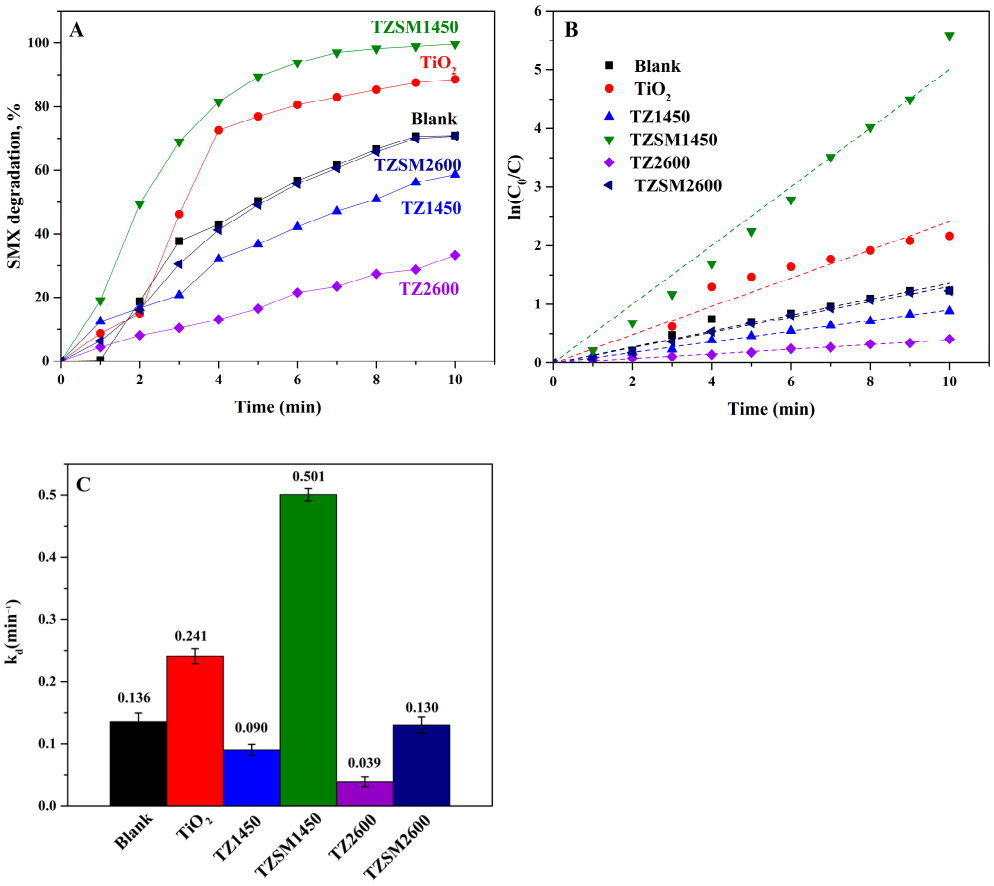

Figure 7. (**A**) SMX degradation for various catalysts, (**B**) kinetic of SMX degradation, and (**C**) degradation pseudo-first-order rate constant (k_d). Conditions: $[SMX]_0$ = 30 mg·L^{-1}, [Catalyst] = 200 mg·L^{-1}.

The photocatalytic degradation of the SMX followed pseudo-first-order kinetics (Figure 7B) with $R^2 > 0.94$ in all cases. The corresponding degradation rate constants (k_d, min^{-1}) followed the order: TZSM1450 > TiO_2 (pure) > TZSM2600 > TZ2450 (Figure 7C). Specifically, the k_d value for the photocatalytic degradation of SMX over TSM1450 was 0.501 min^{-1}, which was 2.08 times the k_d value in the case of pure TiO_2. Yuan et al. [46] reported photocatalytic rate constants in the range of 0.1117–0.5453 min^{-1} for SMX degradation over TiO_2, similar to the one obtained in the present study (0.501 min^{-1}).

TOC removal is an important parameter to assess the ability of a photocatalyst to mineralize a compound. As shown in Figure 8, the conversion of SMX to harmless CO_2, H_2O, and other inorganic species takes longer periods. As for degradation performance, TZSM composites showed better mineralization characteristics than TZ composites (Figure 8A). About 65% and 67% of SMX was mineralized after 120 min by TZSM2600 and TZSM1450, respectively.

The mineralization of the SMX followed pseudo-first-order kinetics too (Figure 8B), as shown by the excellent regression coefficients ($R^2 > 0.96$). The order of the obtained mineralization rate constants (k_m) was TZSM1450 > TZSM2600 > TZ2600 > TZ1450, with their values being 0.0100 min^{-1}, 0.0085 min^{-1}, 0.0020 min^{-1}, and 0.0004 min^{-1}, respectively (Figure 8C).

The effect of common ions like NO_3^-, CO_3^{2-}, and Cl^- was investigated to assess their effect on the activity of TZSM1450 in terms of SMX degradation. The results are shown in Figure 9.

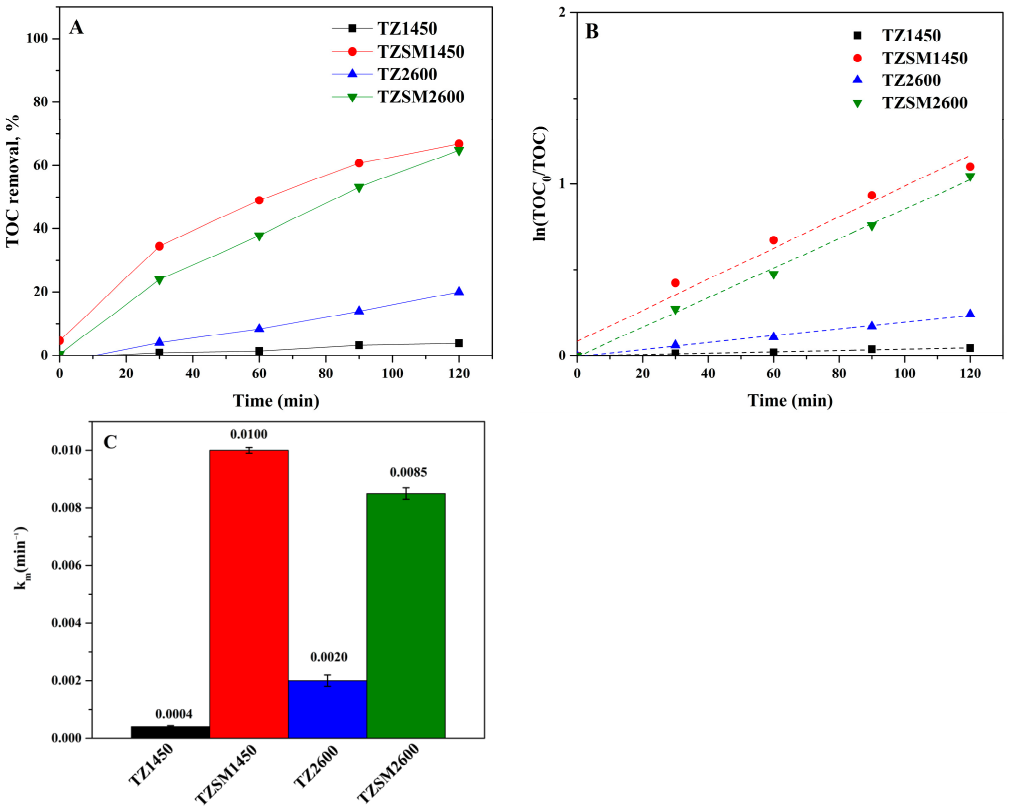

Figure 8. (**A**) TOC removal, (**B**) kinetic of SMX mineralization, and (**C**) mineralization rate constant (k_m). Conditions: $[SMX]_0$ = 30 mg·L^{-1}, [Catalyst] = 200 mg·L^{-1}.

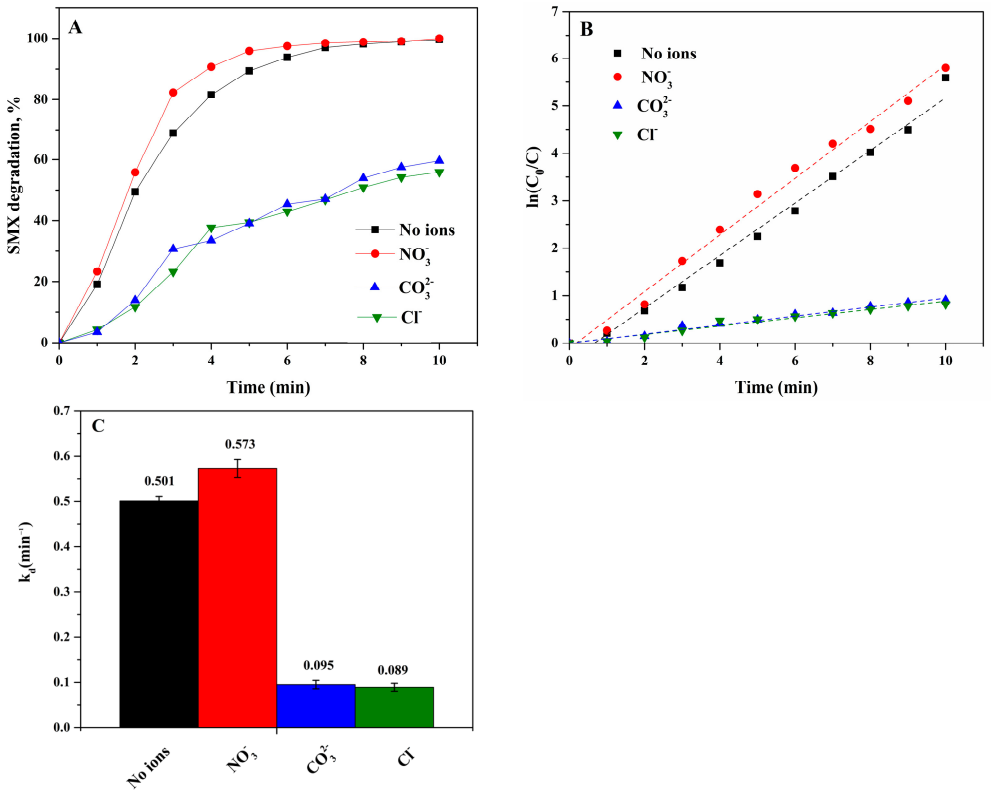

Figure 9. (**A**) The effect of ions (NO_3^-, Cl^-, and CO_3^{2-}) on SMX degradation by UV/TZSM1450, (**B**) kinetic of SMX degradation, and (**C**) degradation rate constant (k_d) in the presence of NO_3^-, Cl^-, and CO_3^{2-}. Conditions: $[SMX]_0$ = 30 mg·L^{-1}, [Catalyst] = 200 mg·L^{-1}.

The coexistence of NO_3^-, CO_3^{2-}, or Cl^- ions in the solution with the concentration of 100 mg·L^{-1} had various effects on the performance of the UV/TZSM1450 system. No remarkable change was observed after the addition of NO_3^- and almost complete SMX degradation was achieved within 10 min. Many studies report the negligible effect of NO_3^- on the photocatalytic degradation of organic pollutants [47–49]. It has to be noted that almost 91% of SMX was degraded after 4 min only in the presence of NO_3^-. This could be associated with the photolysis of NO_3^- (Equations (2)–(7)):

$$NO_3^- \xrightarrow{h\nu} NO_2^- + O \quad (2)$$

$$NO_3^- \xrightarrow{h\nu} O^{\cdot -} + NO_2^{\cdot} \quad (3)$$

$$NO_3^- + H_2O \xrightarrow{h\nu} NO_2^- + OH^- + \cdot OH \quad (4)$$

$$2NO_2^{\cdot} + H_2O \rightarrow NO_2^- + NO_3^- + 2H^+ \quad (5)$$

$$O^{\cdot -} + H_2O \rightarrow \cdot OH + OH^- \quad (6)$$

$$O + H_2O \rightarrow 2\cdot OH \quad (7)$$

On the other hand, CO_3^{2-} and Cl^- ions inhibited the degradation process. The inhibition effect of CO_3^{2-} ions was possibly because the reactive ·OH radicals get scavenged by them [50], and were transformed into the less reactive $CO_3^{\cdot -}$ radicals (Equation (8)):

$$\cdot OH + CO_3^{2-} \rightarrow CO_3^{\cdot -} + OH^- \quad (8)$$

It is worth mentioning that pH can have a deep impact on the formation of radicals [51]. At a highly alkaline pH CO_3^{2-} dominates, while at a low and neutral pH, the carbonate ion will mainly be present in the HCO_3^- form. Both CO_3^{2-} and HCO_3^- react with ·OH by generating $CO_3^{\cdot -}$, however, the reaction between HCO_3^- and ·OH is known to occur more slowly than in the case of CO_3^{2-} and ·OH [52].

Cl^- had the strongest inhibiting effect as a result of the formation of chlorine species (Equations (9)–(16)). These anions may compete with SMX for active sites or also trap active radicals [53], resulting in declined performance [54].

$$Cl^- + \cdot OH \rightarrow Cl^{\cdot} + OH^- \quad (9)$$

$$Cl^- + \cdot OH \rightarrow ClOH^{\cdot -} \quad (10)$$

$$ClOH^{\cdot -} + H^+ \rightarrow Cl^{\cdot} + H_2O \quad (11)$$

$$Cl^- + Cl^{\cdot} \rightarrow Cl_2^{\cdot -} \quad (12)$$

$$Cl_2^{\cdot -} + Cl_2^{\cdot -} \rightarrow Cl_2 + 2Cl^- \quad (13)$$

$$Cl^{\cdot} + Cl^{\cdot} \rightarrow Cl_2 \quad (14)$$

$$Cl_2 + H_2O \rightarrow HOCl + HCl \quad (15)$$

$$HOCl \rightarrow H^+ + ClO^- \quad (16)$$

However, 56% and 60% SMX was still degraded within 10 min in the presence of Cl^- and CO_3^{2-} ions in the solution. The corresponding k_d values in the presence of Cl^- and CO_3^{2-} ions were 0.089 min^{-1} and 0.095 min^{-1}, respectively (Figure 9C).

Figure 10 shows a schematic representation of the photocatalytic degradation of SMX molecules using the TZSM1450 catalyst. The photocatalytic reaction using TZSM1450 was mainly dominated by TiO_2 [32]. Because of the intimate contact between TiO_2 and zeolite [24], electrons (e^-) and holes (h^+) would be formed in the conduction band (CB) and valence band (VB) of TiO_2 under UV light exposure [32,55]. The photo-induced e^- and h^+ migrate to the surface of TiO_2, where they can react with the adsorbed O_2,

while h^+ would oxidize OH^- to produce oxidizing agents like $O_2^{\cdot-}$ and ·OH with high redox potential [56]. However, only around 1% of trapped e^- and h^+ participate in oxidative/reductive processes [57]. Zeolite, applied as a support for TiO_2, can facilitate the efficient delocalization of excited e^- by the electrical conductance between the zeolite and the TiO_2 surface due to the electrical conductance of the zeolites. Thus, the inhibition of charge recombination accounts for the improved photocatalytic activity of the composite photocatalyst [24,58].

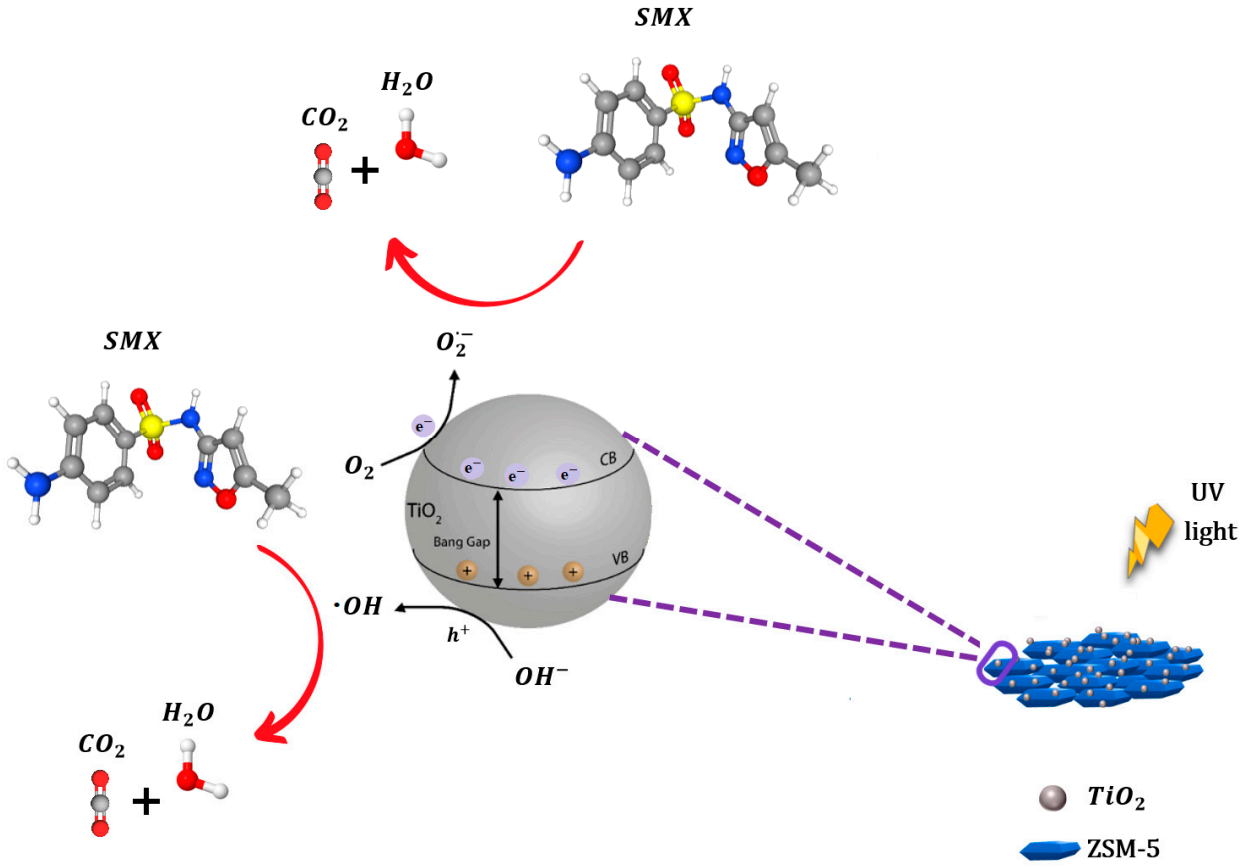

Figure 10. Schematic representation for photocatalytic degradation of SMX by UV/TZSM1450.

2.3. Electrical Energy Estimation

To evaluate the treatment cost of the SMX aquatic solutions by the UV/TZSM1450 process, the electrical energy per order (EE/O) quantity was estimated [59]. Specifically, EE/O was determined as "the electrical energy (kWh) required for the degradation of pollutant by one order of magnitude in 1 m^3 of contaminated water (Equation (17)).

$$EE/O = \frac{P \times t \times 1000}{V \times 60 \times \log\left(\frac{C_i}{C_f}\right)} \quad (17)$$

where P is the power of the lamp (W); t is the photocatalytic reaction time (min); V is the volume of the reactor (L); and C_i and C_f are the initial and final concentrations of SMX, respectively.

The values of EE/O required for the treatment of 1 m^3 of SMX solution were 310.9 kWh m^{-3} $order^{-1}$ for UV only, 177.1 kWh m^{-3} $order^{-1}$ for UV/TiO_2, 434.64 kWh m^{-3} $order^{-1}$ for TZ1450, 68.53 kWh m^{-3} $order^{-1}$ for UV/TZSM1450, 946.48 kWh m^{-3} $order^{-1}$ for UV/TZ2600, and 312.55 kWh m^{-3} $order^{-1}$ for UV/TZSM2600. Thus, the application of UV/TZSM1450 was more attractive in comparison with the other processes considered in this study.

Interestingly, the presence of ions (NO_3^-, CO_3^{2-}, or Cl^-) in the degradation of SMX under UV/TZSM1450 had a diverse effect on the treatment cost. The addition of NO_3^- slightly decreased the electric energy demand from 68.53 kWh m^{-3} $order^{-1}$ to 50.01 kWh m^{-3} $order^{-1}$, while the occurrence of CO_3^{2-} or Cl^- led to the increase of EE/O value to 441.46 kWh m^{-3} $order^{-1}$ and 468.24 kWh m^{-3} $order^{-1}$, respectively.

Since there is a limited number of EE/O studies available for SMX degradation using TiO_2-based photocatalysts, the EE/O values obtained are compared with the ones for other organic pollutants in Table 2. The EE/O values estimated in the present study for SMX degradation are similar to the ones reported by Zambrano et al. [60] using UV/TiO_2.

Table 2. Comparison of EE/O of TiO_2-based photocatalysts for the degradation of various organic pollutants in the literature.

System	Organic Pollutant	Concentration ($mg \cdot L^{-1}$)	Wavelength (nm)/Power (W)	EE/O (kWh m^{-3} $Order^{-1}$)	Ref.
UV/TiO_2	SMX	1	257.7/36	62.1	[60]
UV/TiO_2	Metaldehyde	0.01	253.7/45	4.9	[61]
UV/TiO_2	Cefepime	20	247.3/125	344.09	[62]
UV/TiO_2-Fe-Zeolite/O_3	Sulfoxaflor	100	253.7/38	42.9	[63]
UV/Y-TiO_2-ZSM-5	Methyl orange	8.17	320–440/120	1.56×10^{10}	[64]
UV/TiO_2/ZSM-5	Reactive blue dye (CI250)	10	254/7	74.75	[65]
UV/TZSM1450	SMX	30	365/500	68.53	This work

In addition, the EE/O value for SMX mineralization in the UV/TZSM1450 system was equal to 4156 kWh m^{-3} $order^{-1}$.

3. Materials and Methods

3.1. Materials

Titanium dioxide (TiO_2, P25, 21 nm primary particle size, purity ≥ 99.5% trace metals basis), SMX ($C_{10}H_{11}N_3O_3S$, ≥99%), zeolite with particle size less than 45 μm (Z), sodium nitrate ($NaNO_3$, 99.0%), sodium carbonate (Na_2CO_3, 99.5%), sodium chloride (NaCl, 99.8%), and acetonitrile (CH_3CN, 99.9%) were purchased from Sigma-Aldrich (Waltham, MA, USA St. Louis, MO, USA), while zeolite (ZSM-5) was supplied by ACS Materials (Pasadena, CA, USA). Ultrapure water (UPW (Darmstadt, Germany), 18.25 MΩ*cm) was used for preparing all solutions.

3.2. Preparation of TZ and TZSM Photocatalysts

Two different synthesis methods were used: (1) a simple mechanical mixing method, and (2) a liquid impregnation one. The catalysts were composed of titanium dioxide and zeolite (Z or ZSM-5). The catalysts prepared were labeled as TZxy or TZSMxy depending on whether zeolite Z or ZSM-5 was used, where x and y represent the preparation method and the calcination temperature, respectively.

3.2.1. Preparation of TZ1450 and TZSM1450

TZ1450 and TZSM1450 composites were prepared using a simple mechanical mixing method [66]. Briefly, 1 g of TiO_2 and 5 g of zeolite (Z or ZSM-5) were added to 60 mL of UPW and stirred for 1 h. Then, the mixture was ultra-sonicated for 1 h. The product was dried at 100 °C for 14 h and finally calcined at 450 °C for 8 h. The process is schematically shown in Figure 11.

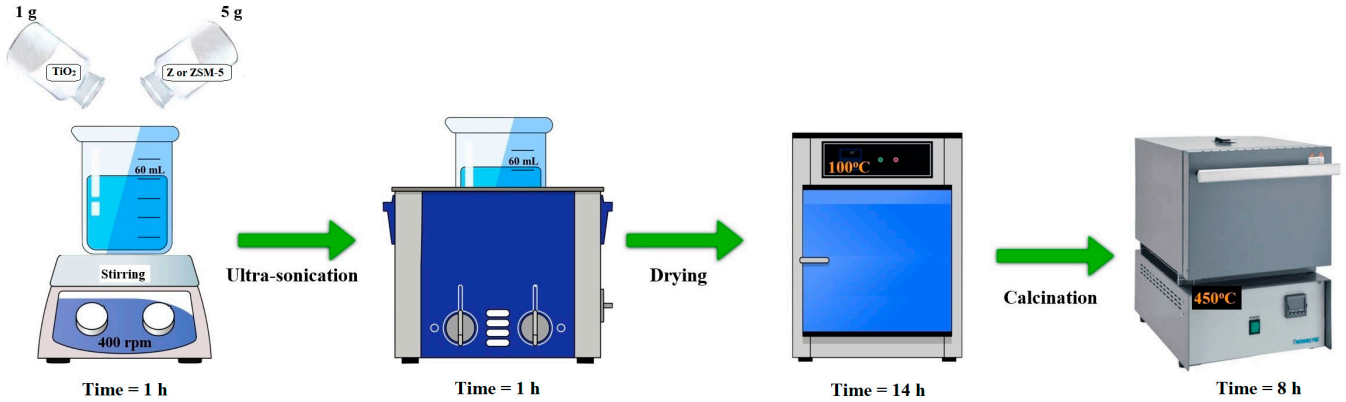

Figure 11. The preparation process for the TZ1450 and TZSM1450.

3.2.2. Preparation of TZ2600 andTZSM2600

TZ2600 and TZSM2600 composites were synthesized using a liquid impregnation method [67]. A total of 4 g of TiO_2 and 1 g of zeolite (Z or ZSM-5) was added to 100 mL of UPW and stirred for 3 h. The resulting precipitate was dried at 100 °C for 14 h, and then calcined at 600 °C for 3 h (Figure 12).

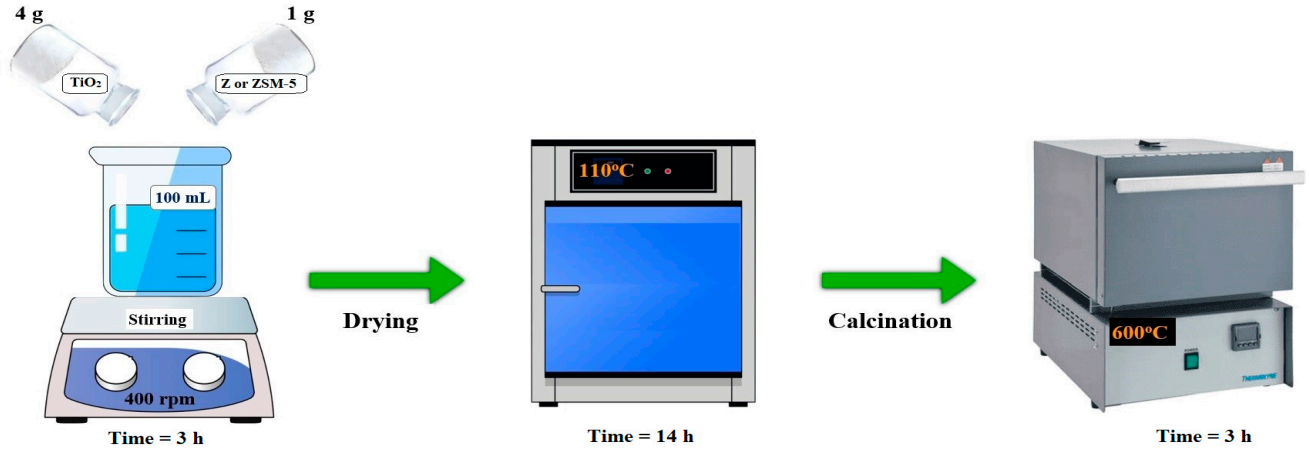

Figure 12. The preparation process for TZ2600 andTZSM2600.

In both approaches, after the calcination step, the homogenization of the resulting precipitate was performed by ball milling for 2 h.

3.3. Characterization

XRD patterns of TZ and TZSM composites were acquired by the X-ray diffractometer (Rigaku Smartlab system, Tokyo, Japan) in a 2θ range of 20–80°, while Raman spectra were recorded using a Raman spectrometer (Horiba, LabRam HR evolution, Kyoto, Japan). SEM images and EDS elemental mapping were obtained by Crossbeam 540 and JSM-IT200 (LA) instruments. DRS spectroscopy was applied to study the optical performance of the composites by diffuse reflectance spectroscopy (DRS, Varian Cary 3, Palo Alto, CA, USA). The specific surface area (S_{BET}) of the composites was determined using an automated gas sorption analyzer (Autosorb iQ, Quantachrome, Boynton Beach, FL, USA) with the BET method.

3.4. Photocatalytic Degradation and Mineralization of SMX

The photocatalytic activity of TZSM1450 and TZSM2600 catalysts was evaluated toward the degradation of SMX under UV light irradiation (365 nm, 500 W) using a photocatalytic reactor (Lanphan industry, Zhengzhou City, China). The photodegradation

process was implemented in a 500 mL reactor. The initial concentrations of SMX solution and catalyst were 30 mg·L^{-1} and 200 mg·L^{-1}, respectively. Before the light irradiation, the solution was stirred magnetically for 30 min in the dark to achieve adsorption–desorption equilibrium. During irradiation, stirring was maintained to keep the mixture in suspension. The whole photocatalytic reaction was maintained at a constant temperature of 25 °C by using a water circulation system. The initial pH of SMX solution was 7.04 and no pH adjustment took place. Approximately 2 mL was taken out every 1 min from the solution to check the SMX degradation and 15 mL was taken every 30 min to check the SMX mineralization. The concentration of SMX was monitored by a high-performance liquid chromatography apparatus (HPLC, Agilent 1290 Infinity II, Santa Clara, CA, USA) equipped with an SB-C8 column (2.1 mm × 100 mm, 1.8 µm) and an ultraviolet detector at a wavelength of 258 nm was used for SMX content analysis. For chromatographic analysis, the injection volume was 1 µL, the flow rate was 0.4 mL/min, and the column temperature was set at 25 °C (both left and right sides) while the retention time was 1.372 min. The mixture of CH_3CN and UPW (40:60 by volume) was used as the mobile phase. The mineralization of SMX was determined by means of a total organic carbon (TOC) analyzer (Multi N/C 3100, Analytic Jena, Jena, Germany).

4. Conclusions

TiO_2/zeolite (TZ and TZSM) composites were synthesized using two different techniques. The photocatalytic performances of the catalysts prepared (200 mg·L^{-1}) were evaluated toward SMX (30 mg·L^{-1}) degradation and mineralization in water under UV light (365 nm) irradiation. The TZSM1450 composite obtained from simple mechanical mixing of TiO_2 with zeolite (ZSM-5), exhibited the best SMX degradation performance among the catalysts investigated in this study, namely 100% SMX degradation within 10 min, which indicated the synergy between TiO_2 and zeolite. Assuming pseudo-first-order rate kinetics, the rate constants were calculated as 0.039, 0.090, 0.130, 0.241, and 0.501 min^{-1} for TZ2600, TZ1450, TZSM2600, TiO_2, and TZSM1450, respectively. The highest TOC removal reached at 120 min was 67% for TZSM1450. The coexistence of Cl^- and CO_3^{2-} exhibited a considerable inhibition effect on SMX degradation, while the presence of NO_3^- had practically no effect on the process. Specifically, the degradation efficiency decreased from 100% to 60% and 56% in the presence of 100 mg·L^{-1} of CO_3^{2-} and Cl^-, respectively. In the case of the TZSM1450 photocatalyst, the electrical energy per order (EE/O) was estimated as 68.53 kWh m^{-3} $order^{-1}$ for SMX degradation and 4156 kWh m^{-3} $order^{-1}$ for SMX mineralization. Finally, the results obtained from this study indicated that the TZSM1450 composite could be a promising catalyst for effective SMX elimination from water.

Author Contributions: Conceptualization, S.G.P., D.M. and T.S.A.; methodology, J.V. and S.M.; investigation, S.M., Z.A. and M.B.; resources, S.G.P., D.M. and T.S.A.; writing—original draft preparation, S.M.; writing—review and editing, S.G.P., T.S.A., J.V. and D.M.; supervision, T.S.A. and S.G.P.; project administration, T.S.A. and S.G.P. All authors have read and agreed to the published version of the manuscript.

Funding: This research was funded by the Science Committee of the Ministry of Science and Higher Education of the Republic of Kazakhstan (Grant No. AP19676347).

Data Availability Statement: Data are contained within the article.

Acknowledgments: The technical support of the Core Facilities of Nazarbayev University is greatly acknowledged.

Conflicts of Interest: The authors declare no conflicts of interest.

References

1. Oh, W.-D.; Dong, Z.; Ronn, G.; Lim, T.-T. Surface–Active Bismuth Ferrite as Superior Peroxymonosulfate Activator for Aqueous Sulfamethoxazole Removal: Performance, Mechanism and Quantification of Sulfate Radical. *J. Hazard. Mater.* **2017**, *325*, 71–81. [CrossRef]

2. Guo, R.; Wang, Y.; Li, J.; Cheng, X.; Dionysiou, D.D. Sulfamethoxazole Degradation by Visible Light Assisted Peroxymonosulfate Process Based on Nanohybrid Manganese Dioxide Incorporating Ferric Oxide. *Appl. Catal. B Environ.* **2020**, *278*, 119297. [CrossRef]
3. Ory, J.; Bricheux, G.; Togola, A.; Bonnet, J.L.; Donnadieu-Bernard, F.; Nakusi, L.; Forestier, C.; Traore, O. Ciprofloxacin Residue and Antibiotic-Resistant Biofilm Bacteria in Hospital Effluent. *Environ. Pollut.* **2016**, *214*, 635–645. [CrossRef]
4. Haenni, M.; Dagot, C.; Chesneau, O.; Bibbal, D.; Labanowski, J.; Vialette, M.; Bouchard, D.; Martin-Laurent, F.; Calsat, L.; Nazaret, S.; et al. Environmental Contamination in a High-Income Country (France) by Antibiotics, Antibiotic-Resistant Bacteria, and Antibiotic Resistance Genes: Status and Possible Causes. *Environ. Int.* **2022**, *159*, 107047. [CrossRef]
5. Wang, J.; Qin, J.; Liu, B.; Song, S. Reaction Mechanisms and Toxicity Evolution of Sulfamethoxazole Degradation by CoFe-N Doped C as Electro-Fenton Cathode. *Sep. Purif. Technol.* **2022**, *298*, 121655. [CrossRef]
6. Doekhi-Bennani, Y.; Leilabady, N.M.; Fu, M.; Rietveld, L.C.; van der Hoek, J.P.; Heijman, S.G.J. Simultaneous Removal of Ammonium Ions and Sulfamethoxazole by Ozone Regenerated High Silica Zeolites. *Water Res.* **2021**, *188*, 116472. [CrossRef] [PubMed]
7. Tang, T.; Liu, M.; Chen, Y.; Du, Y.; Feng, J.; Feng, H. Influence of Sulfamethoxazole on Anaerobic Digestion: Methanogenesis, Degradation Mechanism and Toxicity Evolution. *J. Hazard. Mater.* **2022**, *431*, 128540. [CrossRef]
8. Chen, Y.; Zhang, H.; Xiong, Z.; Wang, Y.; Peng, S.; Wang, J.; Guo, Y. Lithium Cobalt Oxide with Excellent Electron Mobility: An Efficient Activator of Peroxymonosulfate for the Degradation of Sulfamethoxazole. *Chem. Eng. J.* **2022**, *445*, 136702. [CrossRef]
9. Dai, Y.; Cao, H.; Qi, C.; Zhao, Y.; Wen, Y.; Xu, C.; Zhong, Q.; Sun, D.; Zhou, S.; Yang, B.; et al. L-Cysteine Boosted Fe(III)-Activated Peracetic Acid System for Sulfamethoxazole Degradation: Role of L-Cysteine and Mechanism. *Chem. Eng. J.* **2023**, *451*, 138588. [CrossRef]
10. Song, Y.; Zeng, Y.; Liao, J.; Chen, J.; Du, Q. Efficient Removal of Sulfamethoxazole by Resin-Supported Zero-Valent Iron Composites with Tunable Structure: Performance, Mechanisms, and Degradation Pathways. *Chemosphere* **2021**, *269*, 128684. [CrossRef]
11. Bueno, M.J.M.; Gomez, M.J.; Herrera, S.; Hernando, M.D.; Agüera, A.; Fernández-Alba, A.R. Occurrence and Persistence of Organic Emerging Contaminants and Priority Pollutants in Five Sewage Treatment Plants of Spain: Two Years Pilot Survey Monitoring. *Environ. Pollut.* **2012**, *164*, 267–273. [CrossRef]
12. Al Aukidy, M.; Verlicchi, P.; Jelic, A.; Petrovic, M.; Barcelò, D. Monitoring Release of Pharmaceutical Compounds: Occurrence and Environmental Risk Assessment of Two WWTP Effluents and Their Receiving Bodies in the Po Valley, Italy. *Sci. Total Environ.* **2012**, *438*, 15–25. [CrossRef] [PubMed]
13. Yazdanbakhsh, A.; Eslami, A.; Massoudinejad, M.; Avazpour, M. Enhanced Degradation of Sulfamethoxazole Antibiotic from Aqueous Solution Using Mn-WO_3/LED Photocatalytic Process: Kinetic, Mechanism, Degradation Pathway and Toxicity Reduction. *Chem. Eng. J.* **2020**, *380*, 122497. [CrossRef]
14. Liang, D.H.; Hu, Y.; Cheng, J.; Chen, Y. Enhanced Performance of Sulfamethoxazole Degradation Using Achromobacter Sp. JL9 with in-Situ Generated Biogenic Manganese Oxides. *Bioresour. Technol.* **2021**, *333*, 125089. [CrossRef] [PubMed]
15. Nawaz, M.; Khan, A.A.; Hussain, A.; Jang, J.; Jung, H.-Y.; Lee, D.S. Reduced Graphene oxide−TiO_2/Sodium Alginate 3-Dimensional Structure Aerogel for Enhanced Photocatalytic Degradation of Ibuprofen and Sulfamethoxazole. *Chemosphere* **2020**, *261*, 127702. [CrossRef]
16. Mergenbayeva, S.; Atabaev, T.S.; Vakros, J.; Mantzavinos, D.; Poulopoulos, S.G. Photocatalytic Degradation of 4-*Tert*-Butylphenol Using Solar Light Responsive Ag_2CO_3. *Catalysts* **2022**, *12*, 1523. [CrossRef]
17. Mergenbayeva, S.; Kumarov, A.; Atabaev, T.S.; Hapeshi, E.; Vakros, J.; Mantzavinos, D.; Poulopoulos, S.G. Degradation of 4-*Tert*-Butylphenol in Water Using Mono-Doped (M1: Mo, W) and Co-Doped (M2-M1: Cu, Co, Zn) Titania Catalysts. *Nanomaterials* **2022**, *12*, 2326. [CrossRef]
18. Kang, X.; Liu, S.; Dai, Z.; He, Y.; Song, X.; Tan, Z. Titanium Dioxide: From Engineering to Applications. *Catalysts* **2019**, *9*, 191. [CrossRef]
19. Kumarage, G.W.C.; Hakkoum, H.; Comini, E. Recent Advancements in TiO_2 Nanostructures: Sustainable Synthesis and Gas Sensing. *Nanomaterials* **2023**, *13*, 1424. [CrossRef]
20. Wan, X.; Mo, G.; Luo, J. Metal–Organic Frameworks-Derived TiO_2 for Photocatalytic Degradation of Tetracycline Hydrochloride. *Can. J. Chem. Eng.* **2023**, *101*, 1358–1370. [CrossRef]
21. Kamegawa, T.; Kido, R.; Yamahana, D.; Yamashita, H. Design of TiO_2-Zeolite Composites with Enhanced Photocatalytic Performances under Irradiation of UV and Visible Light. *Microporous Mesoporous Mater.* **2013**, *165*, 142–147. [CrossRef]
22. Kovalevskiy, N.S.; Lyulyukin, M.N.; Selishchev, D.S.; Kozlov, D.V. Analysis of Air Photocatalytic Purification Using a Total Hazard Index: Effect of the Composite TiO_2/Zeolite Photocatalyst. *J. Hazard. Mater.* **2018**, *358*, 302–309. [CrossRef]
23. Piedra López, J.G.; González Pichardo, O.H.; Pinedo Escobar, J.A.; de Haro del Río, D.A.; Inchaurregui Méndez, H.; González Rodríguez, L.M. Photocatalytic Degradation of Metoprolol in Aqueous Medium Using a TiO_2/Natural Zeolite Composite. *Fuel* **2021**, *284*, 119030. [CrossRef]
24. You-ji, L.; Wei, C. Photocatalytic Degradation of Rhodamine B Using Nanocrystalline TiO_2–Zeolite Surface Composite Catalysts: Effects of Photocatalytic Condition on Degradation Efficiency. *Catal. Sci. Technol.* **2011**, *1*, 802–809. [CrossRef]
25. Morante-Carballo, F.; Montalván-Burbano, N.; Carrión-Mero, P.; Jácome-Francis, K. Worldwide Research Analysis on Natural Zeolites as Environmental Remediation Materials. *Sustainability* **2021**, *13*, 6378. [CrossRef]

26. Mergenbayeva, S.; Abitayev, Z.; Batyrbayeva, M.; Vakros, J.; Poulopoulos, S.G. Zeolite Supported TiO_2 for the Degradation and Mineralization of Sulfamethoxazole under UV Light Irradiation. *IOP Conf. Ser. Earth Environ. Sci.* **2022**, *1123*, 012086. [CrossRef]
27. Cieśla, J.; Franus, W.; Franus, M.; Kedziora, K.; Gluszczyk, J.; Szerement, J.; Jozefaciuk, G. Environmental-Friendly Modifications of Zeolite to Increase Its Sorption and Anion Exchange Properties, Physicochemical Studies of the Modified Materials. *Materials* **2019**, *12*, 3213. [CrossRef] [PubMed]
28. Sfameni, S.; Rando, G.; Plutino, M.R. Sustainable Secondary-Raw Materials, Natural Substances and Eco-Friendly Nanomaterial-Based Approaches for Improved Surface Performances: An Overview of What They Are and How They Work. *Int. J. Mol. Sci.* **2023**, *24*, 5472. [CrossRef] [PubMed]
29. Faghihian, H.; Bahranifard, A. Application of TiO_2-Zeolite as Photocatalyst for Photodegradation of Some Organic Pollutants. *Iran. J. Catal.* **2011**, *1*, 45–50.
30. Aziztyana, A.; Wardhani, S.; Prananto, Y.; Purwonugroho, D.; Darjito. Optimisation of Methyl Orange Photodegradation Using TiO_2 -Zeolite Photocatalyst and H_2O_2 in Acid Condition. *IOP Conf. Ser. Mater. Sci. Eng.* **2019**, *546*, 042047. [CrossRef]
31. An, Y.; de Ridder, D.J.; Zhao, C.; Schoutteten, K.; Bussche, J.V.; Zheng, H.; Chen, G.; Vanhaecke, L. Adsorption and Photocatalytic Degradation of Pharmaceuticals and Pesticides by Carbon Doped-TiO_2 Coated on Zeolites under Solar Light Irradiation. *Water Sci. Technol.* **2016**, *73*, 2868–2881. [CrossRef]
32. Liu, X.; Liu, Y.; Lu, S.; Guo, W.; Xi, B. Performance and Mechanism into TiO2/Zeolite Composites for Sulfadiazine Adsorption and Photodegradation. *Chem. Eng. J.* **2018**, *350*, 131–147. [CrossRef]
33. Zhang, G.; Song, A.; Duan, Y.; Zheng, S. Enhanced Photocatalytic Activity of TiO2/Zeolite Composite for Abatement of Pollutants. *Microporous Mesoporous Mater.* **2018**, *255*, 61–68. [CrossRef]
34. Li, Y.; Zheng, X.; Guo, Q.; Wang, X.; Zhang, L.; Zhu, W.; Luo, Y. Activation of Peroxymonosulfate by the CoFe/ZSM-5 for Efficient Sulfamethoxazole Degradation. *J. Environ. Chem. Eng.* **2022**, *10*, 107012. [CrossRef]
35. Chi, H.; Wan, J.; Ma, Y.; Wang, Y.; Huang, M.; Li, X.; Pu, M. ZSM-5-(C@Fe) Activated Peroxymonosulfate for Effectively Degrading Ciprofloxacin: In-Depth Analysis of Degradation Mode and Degradation Path. *J. Hazard. Mater.* **2020**, *398*, 123024. [CrossRef] [PubMed]
36. Alvarez, K.M.; Alvarado, J.; Soto, B.S.; Hernandez, M.A. Synthesis of TiO_2 Nanoparticles and TiO_2-Zeolite Composites and Study of Optical Properties and Structural Characterization. *Optik* **2018**, *169*, 137–146. [CrossRef]
37. Aini, N.; Sagita, F.E.; Diyanah, K.; Arifah, A.; Chasanah, S.N.; Prasetyo, A. Structural and Photocatalytic Properties of TiO2/Zeolite Synthesized Using Sol-Gel Method. *Alchemy J. Chem.* **2019**, *7*, 25–30. [CrossRef]
38. Jansson, I.; Suárez, S.; Garcia-Garcia, F.J.; Sánchez, B. Zeolite–TiO_2 Hybrid Composites for Pollutant Degradation in Gas Phase. *Appl. Catal. B Environ.* **2015**, *178*, 100–107. [CrossRef]
39. Xing, S.; Lv, P.; Fu, J.; Wang, J.; Fan, P.; Yang, L.; Yuan, Z. Direct Synthesis and Characterization of Pore-Broadened Al-SBA-15. *Microporous Mesoporous Mater.* **2017**, *239*, 316–327. [CrossRef]
40. Li, X.; Chen, L.; Chen, G.; Zhang, J.; Liu, J. The Relationship between Acidity, Dispersion of Nickel, and Performance of Ni/Al-SBA-15 Catalyst on Eugenol Hydrodeoxygenation. *Renew. Energy* **2020**, *149*, 609–616. [CrossRef]
41. Ahmed, O.; Pons, M.-N.; Lachheb, H.; Houas, A.; Zahraa, O. Degradation of Sulfamethoxazole by Photocatalysis Using Supported TiO2. *Sustain. Environ. Res.* **2014**, *24*, 381–387.
42. Karimi-Shamsabadi, M.; Nezamzadeh-Ejhieh, A. Comparative Study on the Increased Photoactivity of Coupled and Supported Manganese-Silver Oxides onto a Natural Zeolite Nano-Particles. *J. Mol. Catal. Chem.* **2016**, *418–419*, 103–114. [CrossRef]
43. Anandan, S.; Ikuma, Y.; Niwa, K. An Overview of Semi-Conductor Photocatalysis: Modification of TiO_2 Nanomaterials. *Solid State Phenom.* **2010**, *162*, 239–260. [CrossRef]
44. Torkian, N.; Bahrami, A.; Hosseini-Abari, A.; Momeni, M.M.; Abdolkarimi-Mahabadi, M.; Bayat, A.; Hajipour, P.; Amini Rourani, H.; Abbasi, M.S.; Torkian, S.; et al. Synthesis and Characterization of Ag-Ion-Exchanged Zeolite/TiO_2 Nanocomposites for Antibacterial Applications and Photocatalytic Degradation of Antibiotics. *Environ. Res.* **2022**, *207*, 112157. [CrossRef] [PubMed]
45. Duan, X.; Yang, J.; Hu, G.; Yang, C.; Chen, Y.; Liu, Q.; Ren, S.; Li, J. Optimization of TiO2/ZSM-5 Photocatalysts: Energy Band Engineering by Solid State Diffusion Method with Calcination. *J. Environ. Chem. Eng.* **2021**, *9*, 105563. [CrossRef]
46. Yuan, R.; Zhu, Y.; Zhou, B.; Hu, J. Photocatalytic Oxidation of Sulfamethoxazole in the Presence of TiO2: Effect of Matrix in Aqueous Solution on Decomposition Mechanisms. *Chem. Eng. J.* **2019**, *359*, 1527–1536. [CrossRef]
47. Sahoo, C.; Gupta, A.K.; Pal, A. Photocatalytic Degradation of Methyl Red Dye in Aqueous Solutions under UV Irradiation Using Ag+ Doped TiO_2. *Desalination* **2005**, *181*, 91–100. [CrossRef]
48. Wang, C.; Zhu, Q.; Gu, C.; Luo, X.; Yu, C.; Wu, M. Photocatalytic Degradation of Two Different Types of Dyes by Synthesized La/Bi 2 WO 6. *RSC Adv.* **2016**, *6*, 85852–85859. [CrossRef]
49. Shi, W.; Liu, X.; Zhang, T.; Wang, Q.; Zhang, L. Magnetic Nano-Sized Cadmium Ferrite as an Efficient Catalyst for the Degradation of Congo Red in the Presence of Microwave Irradiation. *RSC Adv.* **2015**, *5*, 51027–51034. [CrossRef]
50. Dianati, R.A.; Mengelizadeh, N.; Zazouli, M.A.; Yazdani Cherati, J.; Balarak, D.; Ashrafi, S. Photocatalytic Degradation of Bisphenol A by GO-TiO_2 Nanocomposite under Ultraviolet Light: Synthesis, Effect of Parameters and Mineralisation. *Int. J. Environ. Anal. Chem.* **2022**, 1–18. [CrossRef]
51. Li, J.; Zhang, Q.; Chen, B.; Wang, L.; Zhu, R.; Yang, J. Hydrogen Peroxide Formation in Water during the VUV/UV Irradiation Process: Impacts and Mechanisms of Selected Anions. *Environ. Res.* **2021**, *195*, 110751. [CrossRef] [PubMed]

52. Kumar, A.; Mathur, N. Photocatalytic Degradation of Aniline at the Interface of TiO2 Suspensions Containing Carbonate Ions. *J. Colloid Interface Sci.* **2006**, *300*, 244–252. [CrossRef]
53. Hayati, F.; Isari, A.A.; Anvaripour, B.; Fattahi, M.; Kakavandi, B. Ultrasound-Assisted Photocatalytic Degradation of Sulfadiazine Using MgO@CNT Heterojunction Composite: Effective Factors, Pathway and Biodegradability Studies. *Chem. Eng. J.* **2020**, *381*, 122636. [CrossRef]
54. Wen, X.-J.; Qian-Lu; Lv, X.-X.; Sun, J.; Guo, J.; Fei, Z.-H.; Niu, C.-G. Photocatalytic Degradation of Sulfamethazine Using a Direct Z-Scheme AgI/Bi4V2O11 Photocatalyst: Mineralization Activity, Degradation Pathways and Promoted Charge Separation Mechanism. *J. Hazard. Mater.* **2020**, *385*, 121508. [CrossRef]
55. Joseph, C.; Liew, S.; Bono, A.; Teng, L. Photodegradation of Indigo Dye Using TiO2 and TiO2/Zeolite System. *Asian J. Chem.* **2013**, *25*, 8402–8406. [CrossRef]
56. Yang, L.; Hao, X.; Yu, D.; Zhou, P.; Peng, Y.; Jia, Y.; Zhao, C.; He, J.; Zhan, C.; Lai, B. High Visible-Light Catalytic Activity of Bis-PDI-T@TiO_2 for Activating Persulfate toward Efficient Degradation of Carbamazepine. *Sep. Purif. Technol.* **2021**, *263*, 118384. [CrossRef]
57. Zhao, D.; Sheng, G.; Chen, C.; Wang, X. Enhanced Photocatalytic Degradation of Methylene Blue under Visible Irradiation on graphene@TiO_2 Dyade Structure. *Appl. Catal. B Environ.* **2012**, *111–112*, 303–308. [CrossRef]
58. Mahalakshmi, M.; Vishnu Priya, S.; Arabindoo, B.; Palanichamy, M.; Murugesan, V. Photocatalytic Degradation of Aqueous Propoxur Solution Using TiO2 and Hβ Zeolite-Supported TiO2. *J. Hazard. Mater.* **2009**, *161*, 336–343. [CrossRef]
59. Ma, L.; Yang, Z.; Ji, B.; Liu, Y.; Jiang, Y.; Duan, J.; Zhao, W. Comparative Analysis of Conventional Light Source and LED Array Combined with the Catalyst for Degradation of Antibiotics. *Process Saf. Environ. Prot.* **2021**, *149*, 915–926. [CrossRef]
60. Zambrano, J.; García-Encina, P.A.; Jiménez, J.J.; López-Serna, R.; Irusta-Mata, R. Photolytic and Photocatalytic Removal of a Mixture of Four Veterinary Antibiotics. *J. Water Process Eng.* **2022**, *48*, 102841. [CrossRef]
61. Autin, O.; Hart, J.; Jarvis, P.; MacAdam, J.; Parsons, S.A.; Jefferson, B. Comparison of UV/TiO_2 and UV/H_2O_2 Processes in an Annular Photoreactor for Removal of Micropollutants: Influence of Water Parameters on Metaldehyde Removal, Quantum Yields and Energy Consumption. *Appl. Catal. B Environ.* **2013**, *138–139*, 268–275. [CrossRef]
62. Sahraeian, S.; Alipour, V.; Heidari, M.; Rahmanian, O.; Karimi Abdolmaleki, M. Application of Photocatalytic Process Using UV/TiO2 for Degradation of Cefepime: A Comparison between Photocatalytic and Photolytic. *Iran. J. Chem. Chem. Eng.* **2021**, *40*, 796–803. [CrossRef]
63. Raashid, M.; Kazmi, M.; Ikhlaq, A.; Iqbal, T.; Sulaiman, M.; Zafar, A.M.; Aly Hassan, A. Degradation of Sulfoxaflor Pesticide in Aqueous Solutions Utilizing Photocatalytic Ozonation with the Simultaneous Use of Titanium Dioxide and Iron Zeolite Catalysts. *Water* **2023**, *15*, 1283. [CrossRef]
64. Li, D.; Zheng, H.; Wang, Q.; Wang, X.; Jiang, W.; Zhang, Z.; Yang, Y. A Novel Double-Cylindrical-Shell Photoreactor Immobilized with Monolayer TiO_2-Coated Silica Gel Beads for Photocatalytic Degradation of Rhodamine B and Methyl Orange in Aqueous Solution. *Sep. Purif. Technol.* **2014**, *123*, 130–138. [CrossRef]
65. Subtil, G.W.; Vicentini, J.C.M.; de Oliveira, D.M.; de Castro-Hoshino, L.V.; Yassue-Cordeiro, P.H.; Vicentino, R.C.; Scaliante, M.H.N.O. The Influence of Different Zeolitic Supports on Hydrogen Production and Waste Degradation. *Can. J. Chem. Eng.* **2023**, *101*, 1345–1357. [CrossRef]
66. Saadati, F.; Keramati, N.; Mehdipour Ghazi, M. Synthesis of Nanocomposite Based on Semnan Natural Zeolite for Photocatalytic Degradation of Tetracycline under Visible Light. *Adv. Environ. Technol.* **2016**, *2*, 63–70. [CrossRef]
67. Saqib, N.U.; Adnan, R.; Shah, I. Zeolite Supported TiO_2 with Enhanced Degradation Efficiency for Organic Dye under Household Compact Fluorescent Light. *Mater. Res. Express* **2019**, *6*, 095506. [CrossRef]